Magnetic properties of Dy^{3+} ions and crystal field characterization in YF_3:Dy^{3+} and DyF_3 single crystals

2008 J. Phys.: Condens. Matter 20 485220

(http://iopscience.iop.org/0953-8984/20/48/485220)

J. Phys.: Condens. Matter **20** (2008) 485220 (7pp) doi:10.1088/0953-8984/20/48/485220

Magnetic properties of Dy^{3+} ions and crystal field characterization in YF_3:Dy^{3+} and DyF_3 single crystals

A V Savinkov[1,2], S L Korableva[1], A A Rodionov[1], I N Kurkin[1], B Z Malkin[1], M S Tagirov[1], H Suzuki[2], K Matsumoto[2] and S Abe[2]

[1] Kazan State University, 420008 Kazan, Russia
[2] Kanazawa University, Kakuma-machi, 920-1192 Kanazawa, Japan

E-mail: boris.malkin@ksu.ru

Received 29 June 2008, in final form 4 August 2008
Published 28 October 2008
Online at stacks.iop.org/JPhysCM/20/485220

Abstract

The dc magnetic susceptibilities of the orthorhombic DyF_3 single crystals have been measured in the temperature range between 1.8 and 300 K. The susceptibility along the *b*-axis does not depend on temperature below $T_C = 2.55$ K and is equal to the demagnetizing factor of the sample, that gives evidence for the ferromagnetic phase induced by the magnetic dipole–dipole interactions between the Dy^{3+} ions. The saturation moment of 8.5 μ_B/Dy^{3+} along the *b*-axis was determined from magnetization measurements. The observed strong anisotropy of the magnetic susceptibility at low temperatures agrees with the measured anisotropic *g*-tensor of the ground state of impurity Dy^{3+} ions in YF_3 single crystals. The results of measurements are interpreted in the frameworks of the crystal field theory and the mean magnetic field approximation.

(Some figures in this article are in colour only in the electronic version)

1. Introduction

The heavy-rare-earth trifluorides, from SmF_3 to LuF_3, which belong to the orthorhombic space group *Pnma* (D_{2h}^{16}) [1], show a variety of magnetic behavior and attract interest as model systems for theoretical studies of magnetic ordering in rare earth insulators with competing dipole and exchange interactions. These crystals may be also suitable as potential solid-state laser materials and scintillators. Optical spectra of RF_3 and rare earth doped YF_3:R^{3+} crystals (R = Eu, Tb, Dy, Ho, Er, and Yb) have been measured in [2–6]. Magnetic properties of the heavy-rare-earth trifluorides have been the subject of several studies in the past as well. The ferromagnetic ordering was found from magnetization and specific heat measurements in TbF_3 ($T_C = 3.95$ K [7, 8]) and DyF_3 ($T_C = 2.53$ K [9]). The ground state of the Tb^{3+} ions in TbF_3 is a quasi-doublet with small zero field splitting of ~0.4 cm^{-1} [4]; at low temperatures ($T < T_C$) magnetic moments of the Tb^{3+} ions (~9 in units of the Bohr magneton μ_B) in the two magnetically non-equivalent sublattices are ordered in the *a*–*c* plane at angles $\varphi = \pm 27°$ to the *a*-axis [8]. Due to large values of the magnetic moments, the magnetic ordering is induced mainly by classical dipole–dipole interactions between the terbium ions. Despite a much larger energy gap (6.6 cm^{-1}) between the two lowest crystal field singlet states of the Ho^{3+} ions in HoF_3, the ordered state of the Ho^{3+} magnetic moments (5.7 μ_B) with similar structure (canted ferromagnet, $\varphi = \pm 24°$) was found in HoF_3 ($T_C = 0.53$ K) [10–12]. The antiferromagnetic phase with the magnetic moment of 6.6 μ_B per Er^{3+} ion, lying within the *a*–*c* plane under an angle of 60° from the *a*-axis, was found from the neutron diffraction study in ErF_3 ($T_N = 1.05$ K) [13]. Low temperature magnetic properties of DyF_3 have not been described in the literature; however, the Curie temperature and the direction (*b*-axis) and the value of the spontaneous magnetization (8.4 μ_B per ion) have been communicated [9, 14].

In the present study temperature dependences of the principal values of the magnetic susceptibility tensor in DyF_3 were obtained from measurements of the magnetization in weak external magnetic fields. The ordered state was found

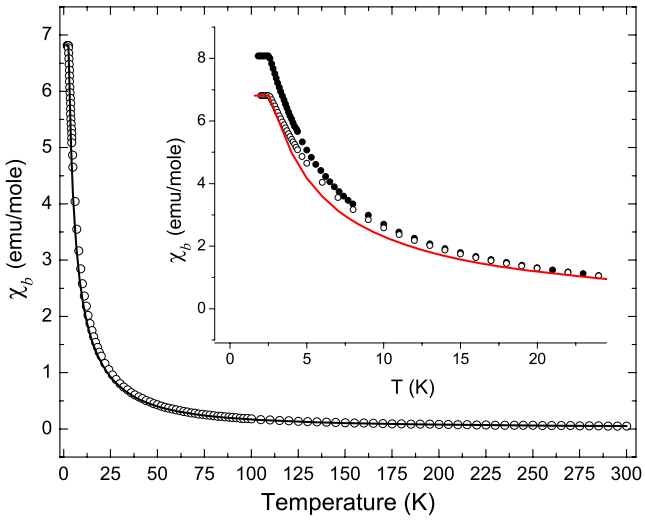

Figure 1. Measured (symbols) and calculated (solid curves, spherical sample) temperature dependences of the static magnetic susceptibility in the magnetic field $\mathbf{B} \parallel b$. Low temperature data for two samples of different shapes (open circles—spherical sample, filled circles—hemispherical sample) are given in the inset.

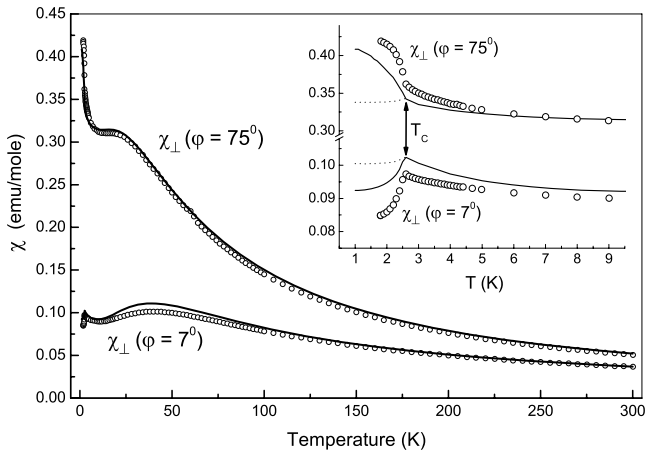

Figure 2. Measured (symbols) and calculated (dotted and solid curves) temperature dependences of susceptibilities in the *ac*-plane (φ is the angle between the magnetic field and the *c*-axis). The low temperature region is enlarged in the inset, where the solid curves represent the results of calculations with the temperature dependent crystal field parameters for $T < T_C$.

at temperatures below $T_C = 2.55$ K. For the magnetic field directed along the *b*-axis, at temperatures $T < T_C$, the susceptibility is determined by the demagnetizing factor of a sample. Such a behavior of the susceptibility gives evidence for the ferromagnetic state induced by the magnetic dipole–dipole interactions between the Dy^{3+} ions. Additional information on the magnetic properties of the Dy^{3+} ions was obtained from low temperature EPR studies of the diluted paramagnet YF_3:Dy^{3+}. The measured components of the *g*-tensor in the ground state of the Dy^{3+} ions and variations of the magnetization in DyF_3 with temperature, magnetic field strength and direction are described in the framework of the crystal field theory. The magnetic dipolar and exchange interactions between the Dy^{3+} ions are considered within the mean-field approximation. Crystal field parameters for concentrated DyF_3 and highly diluted (single ion) YF_3:Dy^{3+} magnets were estimated by making use of the semi-phenomenological exchange charge model [15] and then corrected by comparing the results of calculations with the experimental data.

Computations of crystal field parameters and dipolar magnetic fields were carried out utilizing parameters of the lattice structure obtained from the x-ray diffraction study of the DyF_3 powder at room temperature. The unit cell contains four formula units. Basis vectors $\mathbf{r}_i$ of R^{3+} ions in 4c positions with the point symmetry C_s are (in units of the lattice constants $a = 0.6456$, $b = 0.6909$, $c = 0.4380$ ($\pm 10^{-4}$) nm) $\mathbf{r}_1 = -\mathbf{r}_2 = (u, 1/4, v)$, $\mathbf{r}_3 = -\mathbf{r}_4 = (u - 1/2, 1/4, 1/2 - v)$, the Cartesian coordinates of fluorine F1 ions in 4c positions are determined by parameters u_1 and v_1, and the coordinates of fluorine F2 ions in 8d positions are $\pm(u_2, s_2, v_2)$, $\pm(u_2, 1/2 - s_2, v_2)$, $\pm(u_2 - 1/2, s_2, 1/2 - v_2)$, $\pm(u_2 - 1/2, 1/2 - s_2, 1/2 - v_2)$, where $u = 0.368$, $v = 0.0605$, $u_1 = 0.525$, $v_1 = 0.584$, $u_2 = 0.165$, $s_2 = 0.066$, $v_2 = 0.384$. These structural parameters agree with literature data [13] (ErF_3), [16] (SmF_3, YbF_3) and [17] (TbF_3, HoF_3). Rare earth ions are coordinated by nine fluorine ions: eight ions are at the distances of ~0.23 nm, and one ion is at the distance of ~0.25 nm. The minimal distance between the Dy^{3+} ions equals $r(Dy_1 - Dy_3) = r(Dy_2 - Dy_4) = 0.363$ nm (two neighbors), whereas the next two neighbor Dy^{3+} ions are at the distance of $r(Dy_1 - Dy_2) = r(Dy_3 - Dy_4) = 0.389$ nm.

2. Experimental data

The DyF_3 and YF_3:Dy (0.15 at.%) single crystals were grown by the Bridgman–Stockbarger method in carbon crucibles in an atmosphere of high purity argon from DyF_3 (YF_3) powder at the melting temperature of 1400 °C under an elevated pressure of 200 g cm^{-2}. Additionally, the atmosphere was fluorinated by burning tetra-fluorine-ethylene. A dc-SQUID magnetometer MPMS (Quantum Design) was used for measurements of the magnetization. The axes of the samples were determined using the x-ray technique with an accuracy of ±3°.

We have measured the magnetization $\mathbf{M}(\mathbf{B})$ in the DyF_3 samples at temperatures 1.8–300 K in magnetic fields *B* from 0.1 up to 55 kOe. The temperature dependences of the susceptibilities evaluated from slopes of magnetization curves in the field $B = 100$ Oe for the spherical sample (with approximately 2.1 mm diameter) are shown in figures 1 and 2.

The results of our measurements at temperatures in the range of 80–300 K agree with the data presented in [14]. The principal values of the susceptibility tensor satisfy the inequality $\chi_b > \chi_a > \chi_c$. At low temperatures, the susceptibility becomes extremely anisotropic, being very small in the directions perpendicular to the easy *b*-axis; in particular, χ_b:χ_a:$\chi_c \approx 56$:3.6:1 at the temperature $T = 4.2$ K. The measured angular dependence of the susceptibility $\chi_\perp$ in the *ac*-plane at the temperature of 5 K is presented in figure 3. The

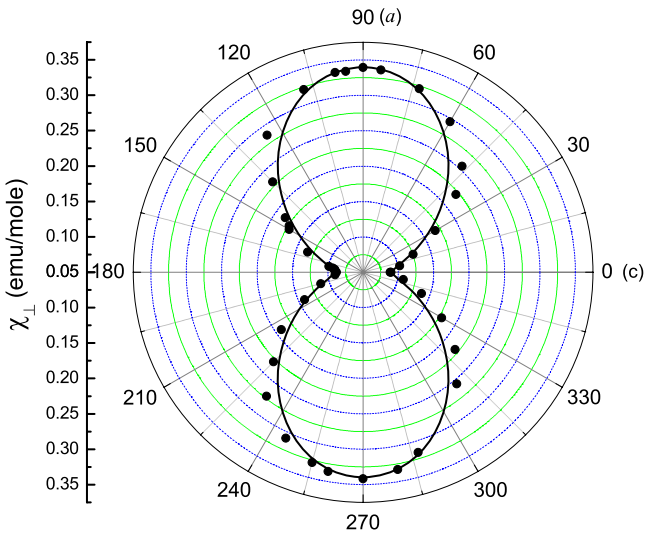

Figure 3. Measured (symbols) and calculated (solid curve) angular dependences of the susceptibility in the *ac*-plane at the temperature of 5 K.

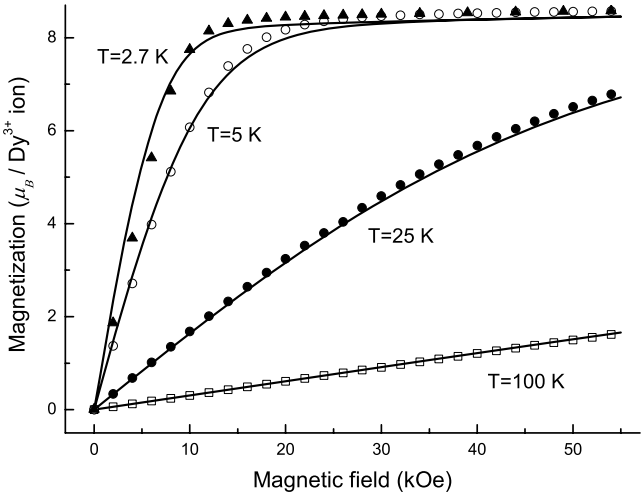

Figure 4. Measured (symbols) and calculated (solid curves) field dependences of the magnetization at different temperatures in magnetic fields **B** ∥ *b*.

temperature variations of the susceptibilities change abruptly at the temperature $T_C = 2.55$ K. Below this temperature, the χ_b susceptibility remains constant, that is a characteristic feature of a dipolar ferromagnet containing domains with zero demagnetizing field. In this case the value of the susceptibility per unit sample mass $\chi_b = (\rho N_b)^{-1}$ at $T < T_C$ along the easy axis is determined by the corresponding demagnetizing factor N_b of the sample (ρ is the mass density) because domains rearrange in the external field B in such a way that the resulting demagnetization field MN_b (here M is the magnetic moment per unit sample volume induced by the external field) compensates exactly the external field. In particular, the measured demagnetizing factor of our spherical sample differs from the demagnetizing factor $4\pi/3$ of the perfect sphere by 2.5% only. The dependence of the susceptibility in the ordered phase on the demagnetizing factor was additionally confirmed by studies of samples with different shapes (see the inset in figure 1).

The χ_c susceptibility exhibits a nonmonotonic temperature dependence (see figure 2). It has a broad maximum at $T \sim 30$ K and a sharp peak at T_C. The temperature behavior of the susceptibility in the *ac*-plane also changes below T_C (see the inset in figure 2); the temperature derivative of the susceptibility $\chi_\perp$ changes continuously from positive to negative values at $T < T_C$ when rotating the magnetic field from the *c*-axis to the *a*-axis.

The magnetic field dependence of the magnetization of the spherical DyF_3 sample along the *b*-axis was measured at temperatures of 2.7, 5, 25 and 100 K (see figure 4). At temperatures close to T_C, the magnetization saturates to 8.5(1) μ_B per Dy^{3+} ion in applied magnetic fields exceeding ∼12 kOe.

Additional information about magnetic properties of the Dy^{3+} ions in trifluorides was obtained from EPR measurements in the YF_3:Dy^{3+} single crystal. The EPR spectra were taken at the frequency of 9.4 GHz and temperatures 5–15 K in constant magnetic fields in the range of 0.05–15 kOe by the continuous wave method with a Bruker ESP-300 X-band EPR spectrometer. Along with strong EPR lines from Dy isotopes with the nuclear spin $I = 0$, rather weak EPR lines with typical hyperfine structure from the ^{161}Dy and ^{163}Dy isotopes (nuclear spin $I = 5/2$) were observed as well (see figure 5). The EPR signals are not observed at temperatures $T > 50$ K due to strong line broadening. For an arbitrary orientation of the field **B**, two resonance lines are observed corresponding to the Dy^{3+} ions in magnetically non-equivalent positions. In the magnetic field directed along the *b*-axis, the EPR spectrum contains a single line corresponding to the *g*-factor $g_b = 16.1$ (see figure 5(a)). For the magnetic field oriented in the *ac*-plane (an example of the spectrum is shown in figure 5(b)), the resonance values of the field strength depend on *g*-factors g_a and g_c and the parameter g_{ac} which is determined below. The values of these parameters (see table 1, column 2) have been obtained from the analysis of the angular dependences of the effective *g*-factors of the magnetically non-equivalent ions, which are shown in figure 6.

Table 1. Components of the *g*-tensor in the ground state of the Dy^{3+} ions.

	YF_3:Dy^{3+}		DyF_3
	Measured	Calculated	Calculated
1	2	3	4
g_a	1.835	1.838	1.002
g_{ac}	0.946	0.894	0.671
g_c	0.550	0.556	0.643
g_b	16.1	16.4	16.25

Thus, due to a large difference between the *g*-factors g_b and g_a, g_c in the ground state of impurity Dy^{3+} ions in YF_3, the concentrated system, DyF_3, may be considered to be an Ising magnet with the easy magnetization direction along the *b*-axis.

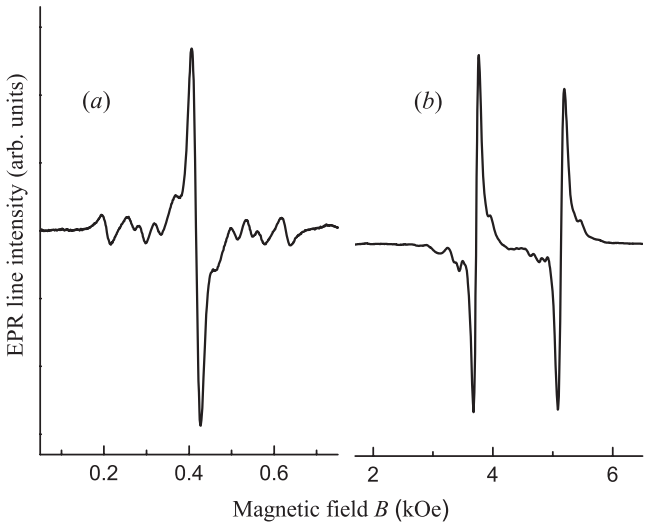

Figure 5. The EPR signals in YF_3:Dy^{3+} at the temperature 15 K in the magnetic fields $\mathbf{B} \parallel b$ (a) and $\mathbf{B} \perp b$ (b).

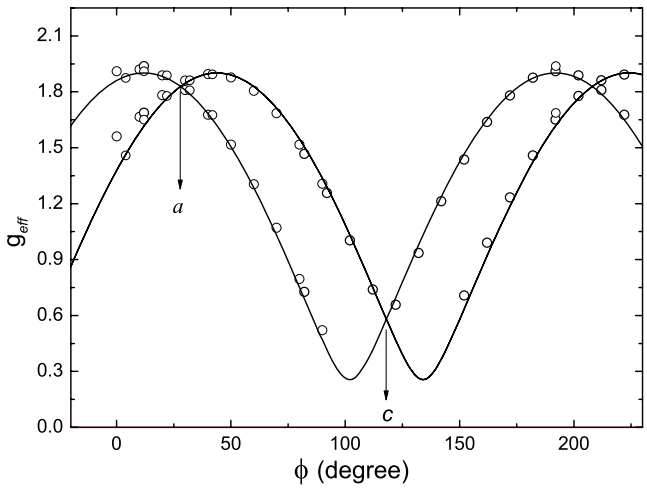

Figure 6. Angular dependences of the effective g-factors in the ac-plane (symbols correspond to the experimental data; the results of calculations are presented by solid curves).

3. Discussion

To describe the results of magnetic and spectral measurements, we consider the effective Hamiltonian of a single Dy^{3+} ion in the j-sublattice, operating in the total basis of 2002 wavefunctions of the electronic $4f^9$ configuration, in the external magnetic field **B**:

$$H_j = H_0 + H_{\mathrm{CF},j} - \boldsymbol{\mu}\mathbf{B}_{\mathrm{loc},j}. \tag{1}$$

Here H_0 is the free ion Hamiltonian with parameters of electrostatic and spin–orbit interactions presented in [18]; $\boldsymbol{\mu} = \mu_{\mathrm{B}} \sum_i (\mathbf{l}_i + 2\mathbf{s}_i)$ is the magnetic moment operator of an ion (the sum is taken over 4f electrons with the orbital **l** and spin **s** moments). The crystal field Hamiltonians

$$H_{\mathrm{CF},j} = \sum_{p=2,4,6} \left[B_p^0(j) C_0^{(p)} + \sum_{k=1:p} B_p^k(j) (C_k^{(p)} + (-1)^k C_{-k}^{(p)}) \right], \tag{2}$$

where $C_k^{(p)}$ are the spherical tensor operators, are determined by a single set of 15 real crystal field parameters (CFPs) $B_p^k(1)$ (we use the Cartesian system of coordinates with the axes x, y, z parallel to the crystallographic axes—c, b, a, respectively, and $B_p^k(1) = B_p^k(2) = (-1)^k B_p^k(3) = (-1)^k B_p^k(4)$; the Dy^{3+} ions in the sublattices 1 and 2, 3 and 4 are magnetically equivalent in pairs). A local magnetic field at the Dy^{3+} ions in sublattice j

$$B_{\mathrm{loc},j\alpha} = B_\alpha + \sum_{i\beta} K_{j\alpha,i\beta} m_{i\beta} \tag{3}$$

(here $\mathbf{m}_i$ is the average magnetic moment of an ion in the sublattice i) is determined by the matrix $K_{i\alpha,j\beta} = Q_{\alpha\beta}(i,j) + J_{\alpha\beta}(i,j) - N_{\alpha\beta}/V$, where $Q_{\alpha\beta}(i,j)$ are the dipolar lattice sums

$$Q_{\alpha\beta}(i,j) = \sum_L \frac{1}{R(0i,Lj)^5} [3R(0i,Lj)_\alpha R(0i,Lj)_\beta - \delta_{\alpha\beta} R(0i,Lj)^2] \tag{4}$$

(the vector $\mathbf{R}(0i,Lj)$ connects the Dy^{3+} ions belonging to the sublattices i and j in the unit cells 0 and L), $J_{\alpha\beta}(i,j)$ are the exchange field parameters, $N_{\alpha\beta}$ are the demagnetizing factors, and V is the unit cell volume. The lattice sums have been computed by the Ewald method and are presented in table 2. To fit the Curie temperature within the mean-field approximation (see below), we introduce the isotropic exchange interaction, $H_{\mathrm{exch}} = -J_{\mathrm{ex}}\mathbf{S}_1\mathbf{S}_2$, between the nearest neighbor Dy^{3+} ions with the spin moments $\mathbf{S}_i$ ($i = 1, 2$), and $J_{\alpha\beta}(1,3) = J_{\alpha\beta}(2,4) = 2(\frac{g_J - 1}{\mu_{\mathrm{B}} g_J})^2 J_{\mathrm{ex}} \delta_{\alpha\beta}$, where $g_J = 4/3$ is the Landé factor for the ground $^6H_{15/2}$ multiplet.

Table 2. Parameters of the dipole–dipole interaction in units of $4\pi/3V$ ($Q_{yz}(i,j) = 0$, $Q_{xy}(i,j) = 0$).

i	j	$Q_{xx}(i,j)$	$Q_{yy}(i,j)$	$Q_{zz}(i,j)$	$Q_{xz}(i,j)$
1	1	2.659 55	0.037 04	0.303 40	0
1	2	−0.276 41	3.030 43	0.245 98	0.113 35
1	3	0.702 30	−1.922 93	4.220 64	0
1	4	0.419 07	2.627 54	−0.046 60	0

The average magnetic moments satisfy the self-consistent equations

$$\mathbf{m}_j = \mathrm{Tr}[\boldsymbol{\mu}\exp(-H_j(\mathbf{m})/k_{\mathrm{B}}T)]/\mathrm{Tr}[\exp(-H_j(\mathbf{m})/k_{\mathrm{B}}T)] \tag{5}$$

(k_{B} is the Boltzmann constant) and are determined in weak magnetic fields by the single ion susceptibility tensors $\boldsymbol{\chi}^{\mathrm{s}}(j)$:

$$m_{j\alpha} = \sum_\beta \chi^{\mathrm{s}}_{\alpha\beta}(j) B_{\mathrm{loc},j\beta} = \sum_\beta \chi^{\mathrm{s}}_{\alpha\beta}(j) \left(B_\beta + \sum_{j\gamma} K_{j\beta,i\gamma} m_{i\gamma} \right). \tag{6}$$

For a given set of CFPs, we calculate components of $\boldsymbol{\chi}^{\mathrm{s}}(j)$ by making use of numerical diagonalization of the Hamiltonian (1). Diagonal components of the single ion susceptibility tensors are the same for all sublattices, $\chi^{\mathrm{s}}_{xy}(j) = \chi^{\mathrm{s}}_{yz}(j) = 0$, and $\chi^{\mathrm{s}}_{xz}(1) = \chi^{\mathrm{s}}_{xz}(2) = -\chi^{\mathrm{s}}_{xz}(3) = -\chi^{\mathrm{s}}_{xz}(4)$. From

equation (6), we obtain the following expression for the bulk susceptibilities:

$$\chi_{\alpha\alpha} = \sum_{ij\beta} X^{-1}_{\alpha\beta}(ij)\chi^{s}_{\beta\alpha}(j),$$
$$X_{\alpha\beta}(ij) = \delta_{\alpha\beta}\delta_{ij} - \sum_{\gamma} \chi^{s}_{\alpha\gamma}(i)K_{i\gamma,j\beta}. \tag{7}$$

In contrast to the single ion susceptibility, the principal axes of the bulk susceptibility tensor coincide with the crystallographic axes. In the magnetic field $\mathbf{B} \parallel y$, all Dy^{3+} ions have the same magnetic moments. The corresponding susceptibility of the spherical sample in the paramagnetic phase is given by

$$\chi_b(T > T_C) = \chi^{s}_{yy}(1) \times \left[1 - \left(\sum_{i=1}^{4} Q_{yy}(1,i) + J_{ex}/8\mu_B^2 - 16\pi/3V\right)\chi^{s}_{yy}(1)\right]^{-1}. \tag{8}$$

Explicit expressions for χ_a and χ_c can be easily obtained from equations (7) (for $\mathbf{B} \parallel x$ or $\mathbf{B} \parallel z$, there are only two independent variables in equation (6), $m_{1x} = m_{3x}$, $m_{1z} = -m_{3z}$, or $m_{1x} = -m_{3x}$, $m_{1z} = m_{3z}$, respectively).

In the ordered ferromagnetic phase, the crystal contains domains with zero demagnetizing factors. The Curie temperature T_C satisfies the following equation, which can be easily obtained from equation (5) for the spontaneous magnetization in such a domain:

$$\left(\sum_{i=1}^{4} Q_{yy}(1,i) + J_{ex}/8\mu_B^2\right)\chi^{s}_{yy}(1,T_C) = 1. \tag{9}$$

We obtain $\chi_b(T_C) = 3V/16\pi$ from equations (8) and (9), and χ_b does not change at temperatures below T_C due to redistribution of domains.

We analyzed the experimental data starting from the initial values of CFP for DyF_3 (see column 2 in table 3) calculated in the framework of the exchange charge model [5, 15]. Then these values were corrected (column 3 in table 3) to fit the measured susceptibilities χ_a and χ_c at low temperatures.

The free ion ground state, $^6H_{15/2}$, is split by the crystal field into eight Kramers doublets, and the gap between the first excited sublevel and the ground doublet exceeds 50 K (see table 4). At liquid helium temperatures most of the Dy^{3+} ions are in the crystal field ground state, and the EPR spectra are described by the projection of the Hamiltonian (1) on the space of wavefunctions $|+\rangle$ and $|-\rangle$ of the ground doublet corresponding to the eigenvalues $\pm 1/2$ of the z-component of the effective spin moment $S = 1/2$. The spin-Hamiltonian of even dysprosium isotopes in YF_3:Dy has the following form:

$$H_S = \mu_B[B_x(g_{xx}S_x \pm g_{xz}S_z) + B_y g_{yy}S_y + B_z(g_{zz}S_z \pm g_{zx}S_x)], \tag{10}$$

where the upper and lower signs refer to the Dy^{3+} ions in the magnetically non-equivalent positions. Components of the g-tensor are $g_{xx} = 2|\langle+|\mu_x|-\rangle|$, $g_{xz} = 2|\langle+|\mu_x|+\rangle|$, $g_{yy} = 2|\langle+|\mu_y|-\rangle|$, $g_{zz} = 2|\langle+|\mu_z|+\rangle|$, $g_{zx} = 2|\langle+|\mu_z|-\rangle|$.

Table 3. Crystal field parameters B^k_p (1) (cm^{-1}) for the Dy^{3+} ions (2—calculated, 3, 5—from the fitting procedure, 4—from [5]).

p	k	DyF_3		YF_3	
	1	2	3	4	5
2	0	290	304	220	299
2	1	−322	−312	−345	−318
2	2	−225	−224	−190	−215
4	0	10	−131	−104	−202
4	1	639	621	687	635
4	2	−16	−29	68	12
4	3	−59	−62	−102	−83
4	4	146	146	28	180
6	0	0	83	−4.8	10
6	1	421	403	365	342
6	2	−539	−523	−367	−555
6	3	39	43	40	41
6	4	−108	−108	−91	−106
6	5	321	315	221	297
6	6	268	276	308	287

The splitting of the ground doublet in the magnetic field, $\Delta\varepsilon(\mathbf{B}) = g_{eff}\mu_B B$, is determined by the effective g-factor

$$g_{eff} = [g_{yy}^2\cos^2\theta + \sin^2\theta(g_c^2\cos^2\varphi + g_a^2\sin^2\varphi \pm g_{ac}^2\sin 2\varphi)]^{1/2}, \tag{11}$$

where θ is the angle between the field $\mathbf{B}$ and the $y(b)$-axis, φ is the angle between the magnetic field projection on the ac-plane and the c-axis, $g_c^2 = g_{xx}^2 + g_{xz}^2$, $g_a^2 = g_{zz}^2 + g_{zx}^2$, $g_{ac}^2 = |g_{zz}g_{xz} + g_{xx}g_{zx}|$.

The set of CFP for YF_3:Dy^{3+} was obtained earlier in [5] from the analysis of optical absorption and luminescence spectra (column 4 in table 3), but the corresponding g-factors of the ground state disagree with the results of EPR measurements described in the preceding section. However, varying CFP obtained from the analysis of the susceptibilities of DyF_3 (column 3 in table 3), we found the set of CFP (column 5 in table 3) close to the starting values that allowed us to describe satisfactorily spectral properties of the diluted YF_3:Dy^{3+} system as well. The calculated g-tensor components of the Dy^{3+} ground state in DyF_3 and YF_3:Dy are compared with the results of measurements in table 1. Not only have g-factors for YF_3:Dy been fitted, but the calculated crystal field energies of sublevels of the ground $^6H_{15/2}$ and excited $^6H_{13/2}$, $^6H_{11/2}$, $^4F_{9/2}$ multiplets also agree satisfactorily with the results of optical studies [5] (see table 4).

A large value of the g-factor g_b is a prerequisite for a dominant role of the dipole–dipole interactions in the ferromagnetic ordering along the b-axis. At low temperatures, the single ion susceptibility can be approximated by the expression $\chi^{s}_{yy}(1) = g_b^2\mu_B^2/4k_BT$, and, from equation (9) with the corresponding lattice sums from table 2 and $J_{ex} = 0$, we obtain the Curie temperature 3.35 K as compared with the observed $T_C = 2.55$ K (the overestimation of the ordering temperature is the inherent property of the mean-field approximation). The exchange-coupling constant, $J_{ex} = -0.067$ cm^{-1} (antiferromagnetic exchange), was adjusted so that the calculated Curie temperature agrees with the observed one.

Table 4. Crystal field energies E_n (cm^{-1}) of the Dy^{3+} ions in YF_3 and DyF_3.

	YF_3		DyF_3		YF_3		DyF_3
Multiplet	Exp. [5]	Calculated	Calculated	Multiplet	Exp. [5]	Calculated	Calculated
1	2	3	4	5	6	7	8
$^6H_{15/2}$	0	0	0	$^6H_{11/2}$	5838	5843	5844
	37	40	42		5862	5866	5863
	59	49	54		5904	5932	5927
	111	107	103		5951	5972	5969
	150	124	122		6034	6049	6049
	211	211	203		6087	6079	6079
	276	279	273				
	502	474	477	$^4F_{9/2}$	21049	21043	21043
					21155	21169	21168
$^6H_{13/2}$	3491	3491	3489		21188	21206	21206
	3546	3560	3560		21267	21279	21277
	3568	3577	3574		21297	21317	21317
	3586	3597	3595				
	3658	3654	3653				
	3762	3753	3753				
	3830	3801	3801				

The single ion magnetic moments $\mathbf{m}(T)$ at different temperatures in the external magnetic field $B = 100$ Oe directed along the crystallographic axes were computed using CFPs from column 3 in table 3. Then the bulk susceptibilities were calculated using equations (7) and the corresponding single ion susceptibilities $\chi^s_{\alpha\beta}(T) = m_\alpha(T)/B_\beta$. As seen in figures 1–3, the calculated temperature and angular dependences of the bulk susceptibilities agree satisfactorily with experimental data in the paramagnetic phase ($T > T_C$). It follows that variations of CFP with temperature in the range of 0–300 K should be rather small.

The observed behavior of the bulk susceptibilities along the a and c axes at low temperatures ($T < T_C$) is the most unexpected result of this work. In the ordered phase, the internal magnetic field along the b-axis, $B_{in} = (\sum_{i=1}^{4} Q_{yy}(1,i) + J_{ex}/8\mu_B^2)m_0(T)$ (m_0 is the spontaneous magnetic moment of a Dy^{3+} ion, which may be assumed to vary with temperature as $|T_C - T|^\beta$, $1/3 < \beta < 1/2$), causes only a small decrease of the susceptibilities in directions normal to the b-axis (see the inset in figure 2, dotted curves) due to splitting of the ground doublet of the Dy^{3+} ions. To describe the increasing (χ_a) and decreasing (χ_c) susceptibilities at low temperatures ($T \to 0$), we have introduced temperature variations of CFP $\Delta B_p^k(j) = a_{pk}(j)[m_0(T)/m_0(0)]^2$ with amplitudes of about ten wavenumbers (in particular, $a_{20}(1) = 20$, $a_{21}(1) = 18$, $a_{22}(1) = 2.5$, $a_{40}(1) = -8$, $a_{44}(1) = 4$, $a_{60}(1) = 3$, $a_{61}(1) = -10$, $a_{65}(1) = -11$, $a_{66}(1) = -5$ cm^{-1}), which may be induced by the spontaneous magnetostriction. This explanation evidently needs additional theoretical or experimental confirmation; however, the detailed discussion of magnetoelastic effects in the title systems is out of the scope of the present work.

The magnetic moments of the Dy^{3+} ions in the magnetic fields along the b-axis at $T > T_C$ were obtained from equation (5) by the method of subsequent approximations; the results of calculations agree satisfactorily with the experimental data (see figure 4).

4. Conclusion

The earlier reported [9] ferromagnetic ordering of DyF_3 along the b-axis has been confirmed and the main governing mechanism of this ordering has been determined. From the direct magnetization measurements, it follows that the ferromagnetic domains are induced at temperatures below $T_C = 2.55$ K due to the magnetic dipole–dipole interactions. The set of CFPs for the Dy^{3+} ions in DyF_3 at the sites with the C_s symmetry has been calculated in the framework of the exchange charge model and corrected to fit the measured susceptibilities, which were analyzed taking into account the classical dipole–dipole and exchange interactions. The constant of the effective antiferromagnetic exchange interaction between the nearest neighbors of -0.067 cm^{-1} has been evaluated within the mean-field approximation; this value is about three times less than the corresponding energy of the dipole–dipole interaction. According to the results of calculations performed with the obtained set of CFPs and confirmed by the EPR measurements in the YF_3:Dy single crystal, the magnetic moment in the ground state of the Dy^{3+} ions is extremely anisotropic, and the DyF_3 crystal may be considered as a quasi-Ising magnet suitable for studies of phase transitions (destructions of the magnetic order) at temperatures below T_C in external magnetic fields normal to the b-axis.

Acknowledgments

This work was supported by the Kazan Federal center for physical and chemical measurements. SLK, INK and BZM acknowledge the support by the Ministry of Science and Education of the Russian Federation (project RNP 2.1.1.7348).

References

[1] Zalkin A and Templeton D H 1953 *J. Am. Chem. Soc.* **75** 2453

[2] Caspers H H, Rast H E and Fry J L 1967 *J. Chem. Phys.* **47** 4505
[3] Kuroda H, Shionoja S and Kushida T 1972 *J. Phys. Soc. Japan* **33** 125
[4] Bumagina L A, Kazakov B N, Malkin B Z and Stolov A L 1977 *Fiz. Tverd. Tela* **19** 1073
Bumagina L A, Kazakov B N, Malkin B Z and Stolov A L 1977 *Sov. Phys.—Solid State* **19** 624 (Engl. Transl.)
[5] Davidova M P, Kazakov B N and Stolov A L 1978 *Fiz. Tverd. Tela* **20** 2391
Davidova M P, Kazakov B N and Stolov A L 1978 *Sov. Phys.—Solid State* **20** 1378 (Engl. Transl.)
[6] Sharma K K, Spedding F H and Blinde D R 1981 *Phys. Rev.* B **24** 82
[7] Holmes L, Guggenheim H G and Hull G W 1970 *Solid State Commun.* **8** 2005
[8] Holmes L and Guggenheim H J 1971 *J. Physique Coll.* **32** 501
[9] Holmes L M, Hulliger F, Guggenheim H G and Maita J P 1974 *Phys. Lett.* A **50** 163
[10] Bleaney B, Gregg J F, Hill R W, Lazzouni M, Leask M J M and Wells M R 1988 *J. Phys. C: Solid State Phys.* **21** 2721
[11] Brown P J, Forsyth J B, Hansen P C, Leask M J M, Ward R C C and Wells M R 1990 *J. Phys.: Condens. Matter* **2** 4471
[12] Leask M J M, Wells M R, Ward R C C, Hayden S M and Jensen J 1994 *J. Phys.: Condens. Matter* **6** 502
[13] Kramer K, Romstedt H, Gudel H U, Fisher P, Murasik A and Fernandez-Diaz M T 1996 *Eur. J. Solid State Inorg. Chem.* **33** 273
[14] Hansen P E, Newald R and Guggenheim H G 1978 *Phys. Rev.* B **17** 2866
[15] Malkin B Z 1987 *Spectroscopy of Solids Containing Rare-Earth Ions* ed A A Kaplyanskii and R M Macfarlane (Amsterdam: Elsevier) pp 13–49
[16] Bukvetskii B V and Garashina L S 1977 *Coord. Chem.* **3** 1024
[17] Piotrowski M, Ptasiewicz-Bak H and Murasik A 1979 *Phys. Status Solidi* a **55** K163
[18] Carnall W T, Goodman G L, Rajnak K and Rana R S 1989 *J. Chem. Phys.* **90** 3443